GDCh Research Article Angewandte International Edition Chemie www.angewandte.org

How to cite: Angew. Chem. Int. Ed. 2025, e202416497
doi.org/10.1002/anie.202416497

CO_2 Conversion Hot Paper

Organoboron-Functionalized Metal-Organic Nanosheets for Highly Efficient CO_2 Fixation Mediated by Frustrated Lewis Pairs

*Cheng-Xia Chen, Haiping Wang, Hassan Rabaâ, Yang-Yang Xiong, Peter VanNatta, Zhang-Wen Wei, Abdullah M. Al-Enizi, Ayman Nafady, and Shengqian Ma**

Dedicated to Professor Hong-Cai Zhou on the occasion of his 60th birthday.

Abstract: Converting CO_2 to high-value fine chemicals represents one of the most promising approaches to combat global warming and subsequently achieve a sustainable carbon cycle. Herein, we contribute an organoboron functionalized ultra-thin metal-organic nanosheet (MON), termed TCPB-Zr-NS, featuring an abundance of exposed Lewis acidic B and formate sites, which can effectively promote CO_2 conversion upon the addition of Lewis basic o-phenylenediamines. Compared with the prototypical 3D analogue TCPB-Zr-3D, the resultant TCPB-Zr-NS showcases dramatically improved catalytic activity for the cyclization of o-phenylenediamine as a result of the highly exposed active sites and efficient substrates/products diffusion. Strikingly, the incorporation of Lewis acidic B sites into ultra-thin Zr-based MON (Zr-MON) not only promotes the highly efficient CO_2 conversion, but also enhances the recyclability/durability of catalysts. Additionally, the underlying catalytic mechanism has been well established by the comprehensive experiments and theoretical calculations, unveiling a formate-assisted frustrated Lewis pairs (FLP) mediated catalytic pathway. This work opens up a new avenue to heterogeneous FLP-based catalysts for small molecule activation and beyond.

Introduction

The conversion of CO_2 to value-added fine chemicals represents one of the most promising methods to combat the global warming and achieve the sustainable carbon cycle.[1–8] In particular, CO_2, serving as an economic, non-toxic, abundant, and recyclable C_1 building block, has been extensively utilized to produce various high-value fine chemicals in organic synthesis, such as cycloaddition of epoxides, propargylic alcohols, or aziridines, and carboxylation of terminal alkyne molecules.[9–16] Thereinto, the cyclization of o-phenylenediamine derivatives with CO_2 has garnered intensive attention due to that the resultant benzimidazoles are a class of ubiquitous motifs in natural products and bioactive molecules, which are widely used in the synthesis of various anticancer agents, antipsychotic drugs, and antimicrobial compounds, *etc.*[17–20] However, the considerable thermodynamic stability and kinetic inertness makes the efficient CO_2 conversion highly challenging.

As a class of important main-group catalyst, frustrated Lewis pairs (FLP), constructed by sterically encumbered Lewis base (LB) and Lewis acid (LA), have attracted enormous attention due to their highly efficient activation performance for small molecules, such as H_2, CO_2, *etc.*, via an environmentally friendly metal-free-mediated catalytic pathway.[21–28] The presence of large steric hindrance confers FLP with great potential for CO_2 activation ascribed to the formation of an active region between Lewis acid and base, where the bonding and antibonding orbitals from CO_2 interact with the vacant orbital of Lewis acid and antibonding orbital of Lewis base, respectively.[29–32] For instance, the Stephan group's groundbreaking demonstration of the concept of FLP for reversible binding of CO_2 under ambient conditions by virtue of $B(C_6F_5)_3$ and $P(t\text{-}Bu)_3$, henceforth paves a brand-new way for CO_2 activation by using FLP catalysts.[33] However, the high sensitivity to moisture for most homogeneous FLPs generally results in dramatically reduced catalytic efficiency and poor reusability. Additionally, the homogeneous systems intrinsically result in a greatly increased separation complexity when compared with heterogeneous systems. Therefore, it is highly desirable yet challenging to develop heterogeneous FLP catalysts with excellent stability and high catalytic activity.

The significant progress of FLP catalysis to date has fully taken advantage of the combination of various Lewis acids and Lewis bases, which in turn propels the FLP chemistry into a new realm for constructing heterogeneous FLP

[*] Dr. C.-X. Chen, H. Wang, Dr. H. Rabaâ, Dr. P. VanNatta, Prof. S. Ma
Department of Chemistry, University of North Texas CHEM 305D. 1508 W Mulberry St, Denton, Texas 76201, United States
E-mail: shengqian.ma@unt.edu

Dr. C.-X. Chen, Dr. Y.-Y. Xiong, Dr. Z.-W. Wei
MOE Laboratory of Bioinorganic and Synthetic Chemistry, GBRCE for Functional Molecular Engineering, Lehn Institute of Functional Materials, IGCME, School of Chemistry, Sun Yat-Sen University, Guangzhou 510006, China

Dr. H. Rabaâ
Department of Chemistry, Ibn Tofail University, ESCTM, P.O. Box 133, 14000, Kenitra, Morocco

Prof. A. M. Al-Enizi, Prof. A. Nafady
Department of Chemistry, College of Science, King Saud University Riyadh, 11451, Saudi Arabia

catalysts as an alternative to improve the homogeneous FLP catalyst's stability, product/catalyst separation, and catalyst recycling.[34–39] In this vein, many research groups have developed a series of FLP-functionalized metal–organic frameworks (MOFs) (FLP-MOFs) through sequentially dynamic installation of Lewis base and Lewis acid into the prototypical MOF or *de novo* synthesis, which display efficient catalytic activity and good recyclability.[35–36,40–45] Among these works, it should be noted that the distance between LA and LB is of great importance for the catalytic efficiency which can be achieved through regulating steric hindrance of LA and LB or immobilizing them in specifically spatial location of the MOF matrix. For instance, Deng and co-workers reported a series of FLP MOFs with both LA and LB fixed in the MOF skeleton through geometry restriction, wherein the distance and location of LA and LB can be precisely regulated, thus providing a platform to investigate influences from the electrostatic effect and distance to the catalytic performance of FLP.[36] Nevertheless, rigorously controlled environments and complex operating procedures are still required, usually in a glovebox to preclude the attack of water and oxygen, for the synthesis of FLP-MOFs and subsequent execution of the catalytic reactions to achieve good catalytic efficiency and recyclability. Moreover, the introduction of larger FLP active sites into MOFs hinders the substrates/products diffusion in the MOF pores/channels with limited sizes (typically < 2 nm) and the access of substrates to the catalytic centers, resulting in unsatisfactory catalytic efficiency in comparison with the homogeneous FLP counterparts.

Metal-organic nanosheets (MONs), serving as a class of two-dimensional versions of MOFs with one dimension reduced to nanometer scale in thickness, have gathered extensive attention in the field of catalysis.[46–51] Due to the large specific surface area, ultrathin thickness, and high surface-to-volume atom ratios, subtle design and selection of organic linkers and metal ions (clusters) can enable MONs with targeted functionality, involving an abundance of exposed active sites, and free substrates access to the active sites, thus providing a brand-new heterogeneous platform for highly efficient catalysis.[46,49,51] Recently, Zr-MONs based on the ultra-strong Zr–O coordination bond have aroused enormous research interest due to their high thermal and chemical stability.[52–55] Organoboron functionalized linkers have been widely used to design and assembly versatile electron-deficient functional materials,[56–57] in which the organoborane linkers sterically protected by bulk aryl groups can serve as Lewis acidic sites to react with a Lewis base to form FLP due to its unique ground state electron configuration, $1s^2 2s^2 2p^1$, and vacant *2p* orbital in the valence shell, thus endowing the assembled framework materials with unique catalytic properties in heterogeneous catalysis. Additionally, the bulky hydrophobic duryl group can effectively protect the Lewis acidic boron (B) sites from the strong attack of small donor molecules like H_2O, thus enhancing the stability of active sites. Along this line, we anticipate that incorporating the organoboron functionalized linkers into Zr-MONs will not only confer desired features including high stability, abundance of exposed active sites, and specific catalytic activity from their parent species, but also bestow the resultant materials with superior catalytic activity and excellent recyclability that their prototype counterparts can hardly achieve.

Herein, we developed a robust organoboron functionalized Zr-MONs, termed TCPB-Zr-NS, featuring an abundance of highly exposed Lewis acidic B and formate sites, constructed from the organoborane linkers, (tris((4-carboxyl)phenylduryl)borane, TCPB), with $ZrCl_4$, for highly efficient CO_2 fixation by means of *in situ* formation of FLP. Compared with the prototypical TCPB-Zr-3D, the resultant TCPB-Zr-NS presents dramatically improved catalytic performance for the conversion of o-phenylenediamines to high-value benzimidazole derivatives by using CO_2 as a C_1 source attributed to the high exposed active B sites, formates, and efficient substrates/products diffusion. Notably, the incorporation of Lewis acidic B sites into TCPB-Zr-NS not only promotes the efficient CO_2 chemical fixation, but also greatly improves the stability/durability of the framework as confirmed by the consecutive catalytic reactions operated under ambient conditions. Moreover, the underlying catalytic mechanism has been well established by comprehensive experiments and theoretical simulations, demonstrating a formate-assisted FLP-mediated catalysis pathway.

Results and Discussion

The TCPB-Zr-3D of composition $Zr_6(\mu_3\text{-}O)_4(\mu_3\text{-}OH)_4\text{-}(TCPB)_2(HCOO)_6$ was synthesized through the solvothermal reaction of TCPB with $ZrCl_4$ in *N,N'*-dimethylformamide (DMF) solution at 120 °C for 168 h using formic acid (FA) as the modulator (Figure S3). Single-crystal X-ray diffraction (SCXRD) analysis reveals that TCPB-Zr-3D crystalizes in *C*2/*m* space group (Table S1). There are two thirds of TCPB linker, one third of Zr_6 cluster, and one and a half of formate molecules in the asymmetric unit. Notably, for each Zr_6 cluster, four formate molecules coordinate to the out of plane binding sites on the Zr_6-clusters as the terminal carboxylates, while the other four formate molecules connect the adjacent Zr_6-clusters as the bridging ligands (Figure 1a–d, S3). Every Zr_6-cluster is coordinated by six TCPB linkers, while every TCPB ligand is connected by three Zr_6-clusters, thus forming a 2D (3,6)-connected layer network, which is further connected by formate to form the final 3D networks (Figure 1c, d). TCPB-Zr-3D features two kinds of channels, i.e., one rectangular channel with the aperture size of ca. 8.0×10.8 Å^2, and one rhombic channel with the pore size of ca. 4.0×13.2 Å^2 along the *c*-axis, respectively (Figures 1d, S1). TCPB-Zr-3D is constructed by the 2D layer network which is vertically bridged by the formate groups (Figure 1c, enlarged part), thus imposing the potential for transforming the parent 3D network to 2D layer, and tuning the interlayer spacing via substituting the terminal and bridged formate groups by water.

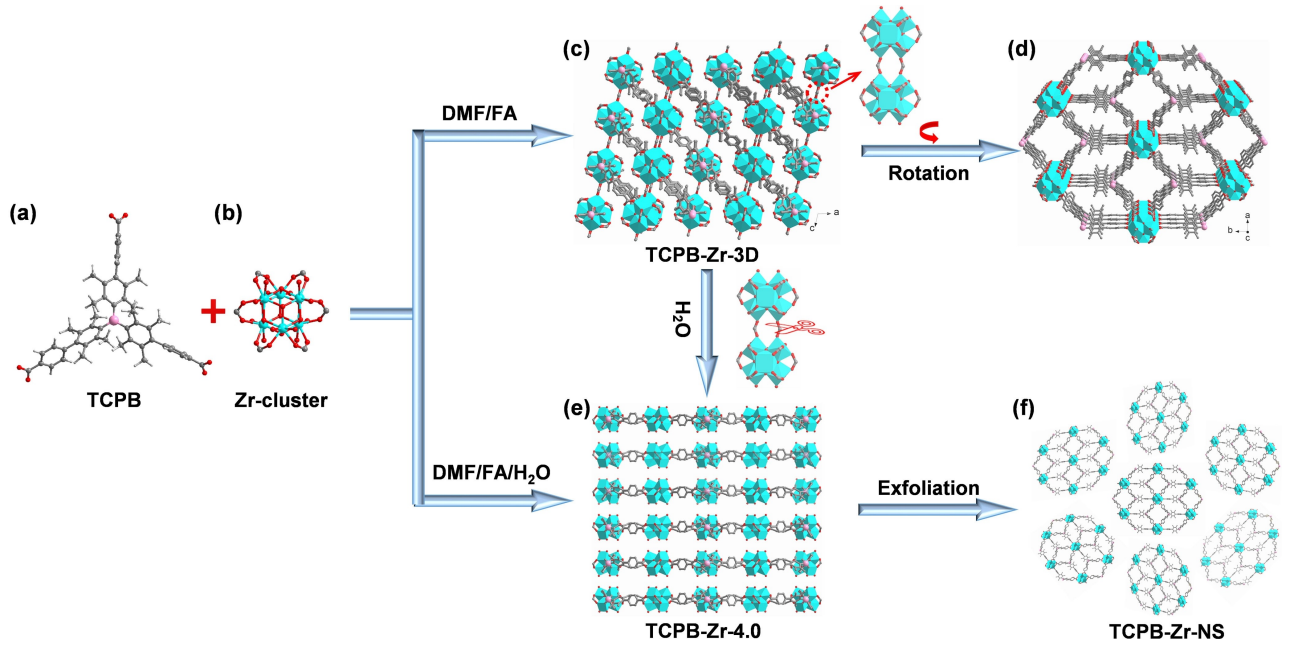

Figure 1. The schematic synthetic route of TCPB-Zr-NS. (a) TCPB ligand; (b) Zr_6 cluster; the structure of TCPB-Zr-3D showing (c) layers and (d) channels, respectively; the structure of (e) TCPB-Zr-4.0 and (f) TCPB-Zr-NS.

To probe the effect of water on the structure of TCPB-Zr-3D, featuring a blocky morphology, a series of control experiments were executed wherein different amounts of water were added to the synthesis system, demonstrating that a series of 2D lamellar structures have been gained, termed TCPB-Zr-x, (× (mL) represents the amount of water used in the synthesis process), revealed by the scanning electron microscope (SEM) measurements (Figure S6). Notably, the sample thickness gradually decreases along with the increased water dosage amounts from 0 to 4.0 mL which we ascribe to the gradually increased substitution of bridged formate groups by the water molecules, confirmed by the SEM images and ^{1}H NMR spectra (Figures S4, S6). Le Bail refinement manifests that TCPB-Zr-4.0 crystalizes in the orthorhombic *Imma* space group (Figure S2). TCPB-Zr-4.0 possesses a 2D network with Zr_6 clusters ligated by six independent TCPB linkers and five terminal formates (Figure S5), while each TCPB linker is connected by three Zr_6 clusters, thus resulting in an isostructure of Zr-BTB (BTB = 1,3,5-tris(4-carboxyphenyl)benzene) (Figure 1e).[50,54,58–59] Notably, continuously increasing the dosage of water to 4.5 mL will lead to the formation of a stick-like impurity (Figure S6). Therefore, TCPB-Zr-4.0 was determined to be the best recipe to produce the targeted nanosheets. As shown in Figure S6, TCPB-Zr-4.0 features a distinct nano-flower morphology, comprised of multiple closely packed lamellae, which can be exfoliated into ultra-thin nanosheets, termed TCPB-Zr-NS, through ultrasound-assisted liquid phase stripping (Figure 1f). The Tyndall scattering experiment was performed for the colloid solution of TCPB-Zr-NS, in which an obvious Tyndall effect is observed without precipitate found, confirming the successful exfoliation (Figure 2a, inset). The high-resolution transmission electron microscope (HR-TEM) images further unveil the wrinkled and ultra-thin morphology of TCPB-Zr-NS (Figure 2a–d). To assess the thickness of TCPB-Zr-NS, the atomic force microscope (AFM) was used to reveal that the thickness of TCPB-Zr-NS is ~3.2 nm in size, corresponding to approximately bilayer (Figure 2f, g). Moreover, the images of element mapping were conducted to confirm the even distribution of C, O, Zr, and B throughout the TCPB-Zr-NS framework (Figure 2e). Importantly, the ultra-thin 2D structure bestows TCPB-Zr-NS with highly exposed Lewis acidic sites, i.e. B atoms, which are protected by bulky hydrophobic duryl groups for preventing the strong interactions between B and other small donor molecules, such as H_2O, from occurring, thus imposing significantly enhanced catalytic potential via FLP-mediated pathway compared with the prototypical TCPB-Zr-3D.

The phase purity for TCPB-Zr-3D, TCPB-Zr-x, and TCPB-Zr-NS were confirmed by powder X-ray diffraction (PXRD) patterns (Figures 3a, S7–S8). The thermal stabilities were evaluated by thermogravimetric analyses, revealing that TCPB-Zr-3D, TCPB-Zr-4.0, and TCPB-Zr-NS can be stable up to 400 °C (Figure S10). The porosity for all the synthesized samples were assessed by the N_2 adsorption isotherms at 77 K (Figures 3b, S11). Compared with TCPB-Zr-3D (151 $cm^3 g^{-1}$ and 324 $m^2 g^{-1}$), TCPB-Zr-4.0 presents much higher N_2 uptakes with the value of 345 $cm^3 g^{-1}$, corresponding to the BET surface area (S_{BET}) of 1029 $m^2 g^{-1}$, due to the exposure of more accessible surface ascribed to the removal of the bridging formate groups resulting in reduced layer thickness (Table S2). Notably, TCPB-Zr-NS shows a type II adsorption isotherm in contrast with its prototypical counterpart, TCPB-Zr-4.0, featuring a type I adsorption isotherm, suggesting the further expansion of the

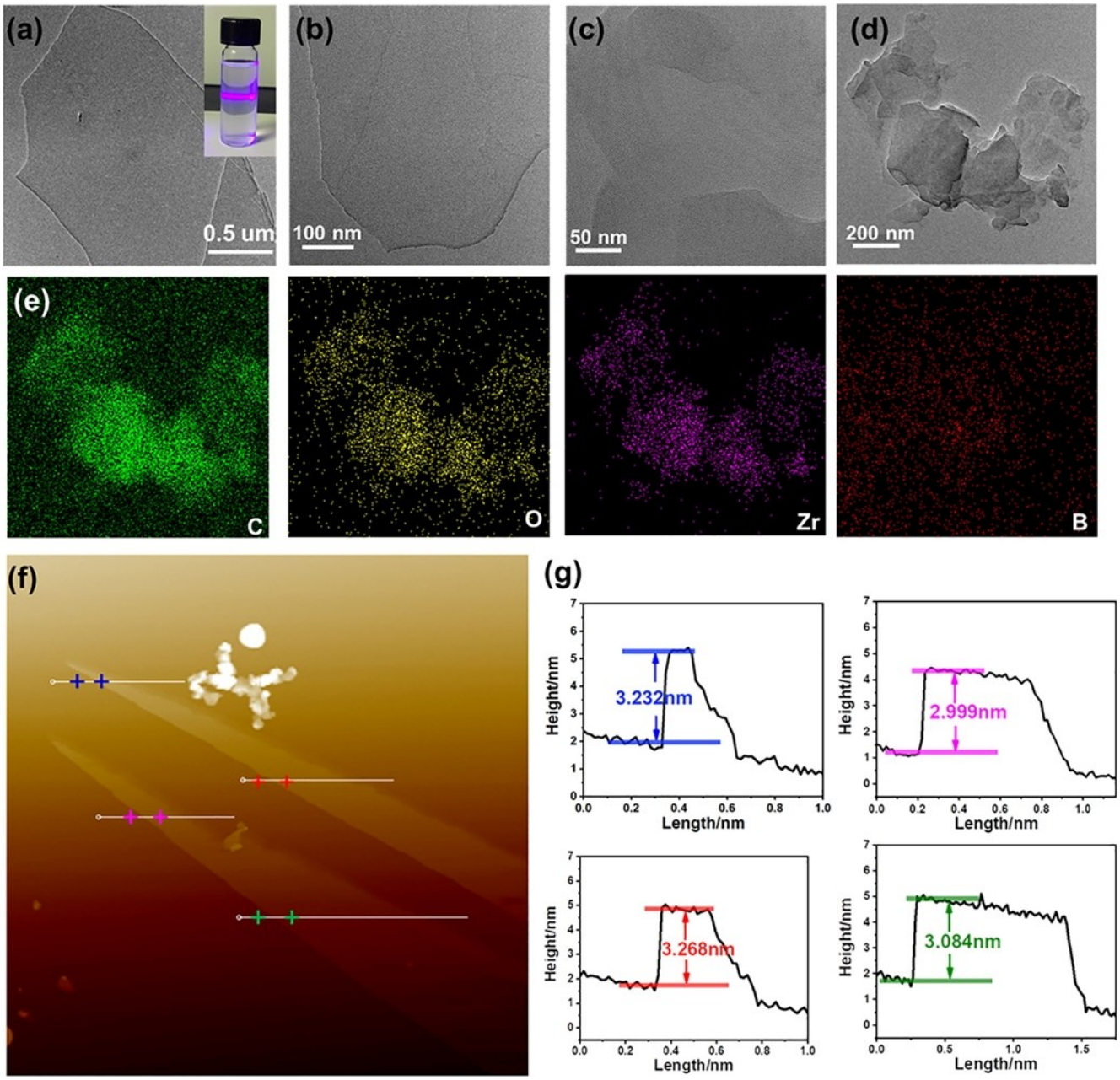

Figure 2. (a–d) The HR-TEM images of TCPB-Zr-NS, inset represents the Tyndall effect of TCPB-Zr-NS dispersed in ACN; (e) the elemental mappings of C, O, Zr, and B for TCPB-Zr-NS; (f) the AFM image of TCPB-Zr-NS; (g) the corresponding height curves for the selective areas in part.

layer spacing (Figure 3b). The N_2 uptake capacity of TCPB-Zr-NS is 403 $cm^3 g^{-1}$, corresponding to the S_{BET} and pore volume of 471 $m^2 g^{-1}$ and 0.62 $cm^3 g^{-1}$, respectively (Table S2).

The cyclization of o-phenylenediamine with CO_2 is chosen to evaluate the catalytic potential of TCPB-Zr-NS as the produced benzimidazole derivatives are an important class of molecules with pharmacological and biological activity (Table 1, S3). Initially, the reaction was tested between commercial o-phenylenediamine and CO_2 with hydrosilane as the reductant and TCPB-Zr-NS as the catalyst in a polytetrafluoroethylene (PTFE)-lined autoclave, revealing that TCPB-Zr-NS can drive the cyclization reaction. The effect of organic solvents was firstly surveyed by using Ph_2SiH_2 as the reductant under 1 MPa CO_2 pressure at 120 °C for 24 h, in which the cyclization reaction proceeded most smoothly in acetonitrile (ACN) solution, with a yield of 89 % (Table 1, Entry 1, 2, and 3). Whereafter, the influence of the amount of Ph_2SiH_2 on the reaction was examined, which showed that the yield of benzimidazole gradually improved from 33 to 82 % with increasing the amount of Ph_2SiH_2 from 1 to 4 equivalent, indicating the importance of the reducing agent on the reaction (Table 1, S3). The yield of benzimidazole decreased from 89 to 82 %

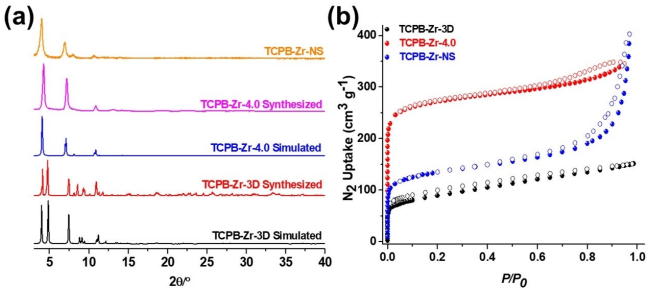

Figure 3. (a) The PXRD patterns of TCPB-Zr-3D, TCPB-Zr-4.0, and TCPB-Zr-NS; (b) the N_2 adsorption isotherms of TCPB-Zr-3D, TCPB-Zr-4.0, and TCPB-Zr-NS at 77 K.

Table 1: The optimization of cyclization reaction.[a]

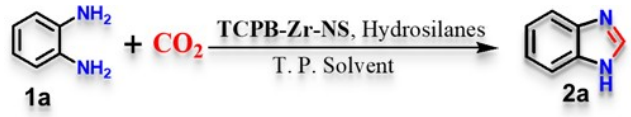

Entry	Hydrosilane (eq.)	Solvent	TCPB-Zr-NS (mol%)	Yield (%)
1	Ph_2SiH_2 (4)	ACN	6.2	89
2	Ph_2SiH_2 (4)	THF	6.2	61
3	Ph_2SiH_2 (4)	Toluene	6.2	40
4[b]	Ph_2SiH_2 (1)	ACN	4.2	33
5[c]	Ph_2SiH_2 (4)	ACN	4.2	82
6[d]	Ph_2SiH_2 (4)	ACN	6.2	78
7[e]	Ph_2SiH_2 (4)	ACN	6.2	78
8[f]	Ph_2SiH_2 (4)	ACN	6.2	91
9	$PhSiH_3$ (4)	ACN	6.2	99
10[g]	$PhSiH_3$ (4)	ACN	6.2	59

[a] The reactions were performed in a PTFE-lined autoclave (20 mL) with 1a (0.2 mmol), hydrosilane (0.8 mmol), and TCPB-Zr-NS (6.2% mol, based on B centers) in solvent (2.0 mL) under CO_2 (1.0 MPa) atmosphere; [b] Ph_2SiH_2: 1 equiv, Catalyst loading: 4.2%; [c] Ph_2SiH_2: 4 equiv, Catalyst loading: 4.2%; [d] CO_2 pressure: 0.5 MPa; [e] Reaction temperature: 80 °C; [f] Reaction temperature: 140 °C; [g] Catalyst: TCPB-Zr-3D.

along with the reduced catalyst quantity from 6.2 to 4.2% (Table 1, Entry 1 and 5). The optimization of CO_2 pressure was performed, which revealed that the yield decreased from 89 to 78% with reducing the CO_2 pressure from 1 to 0.5 MPa (Table 1, Entry 1 and 6). Lowering the reaction temperature from 120 to 80 °C resulted in the dramatically decreased cyclization yield from 89 to 78%, whereas elevating the reaction temperature from 120 to 140 °C gave rise to a slight increase in yield from 89 to 91% (Table 1, Entry 1, 7, and 8). Further optimization revealed that $PhSiH_3$ (99%) presented better efficacy on the reaction than Ph_2SiH_2 (89%) (Table 1, Entry 1 and 9). Noteworthily, the cyclization proceeded poorly in absence of TCPB-Zr-NS, suggesting the pivotal role of TCPB-Zr-NS (Table S3, Entry 11). Additionally, the porotype TCPB-Zr-3D showed dramatically decreased yield of benzimidazole (59%) compared with TCPB-Zr-NS (99%), indicative of the significantly improved catalytic activity for TCPB-Zr-NS stemming from the highly exposed active sites and fast substrates/products diffusion (Table 1, Entry 9 and 10).

Having identified the optimized condition, the substrate scope of the cyclization reaction was examined. As depicted in Table 2, TCPB-Zr-NS presented good catalytic activity towards a variety of electron-rich and -poor o-phenylenediamines, with the yields of benzimidazole derivatives from moderate to high. Notably, the electron effect of the substituted o-phenylenediamines had a remarkable impact on the cyclization reaction, in which the electron-rich o-phenylenediamine performed smoothly to give the corresponding product (**2b**) in 99% yield, whereas the electron-poor o-phenylenediamines furnished the corresponding products in a yield range of 61–83% (**2c**, **2d**) following the trend of –Cl > –NO_2. Additionally, the 3,4-difluoride and pyridine-substituted diamines resulted in the corresponding benzimidazoles **2e**, **2f**, with good yields of 96 and 73%, respectively. The cyclization of naphthalene-based diamine (**1g**) with CO_2 proceeded smoothly, affording 1*H*-naphtho-[2,3-*d*] imidazole (**2g**) in an 89% yield, whereas the naphthalene-1,8-diamine was transformed to 1H-perimidine (**2i**) in a moderate yield (42%). In addition, the *N*-phenyl-substituted o-phenylenediamine furnished the corresponding product (**2h**) with a yield of 83%. Noteworthily, TCPB-Zr-NS presents much higher yields of **2g** and **2h** than the prototype TCPB-Zr-3D (**2g**: 19%; **2h**: 36%), further demonstrating the outstanding catalytic performance of TCPB-Zr-NS featuring the highly exposed active sites and fast substrates/products diffusion ability (Table 2). To assess the recyclability and durability of TCPB-Zr-NS, consecutive experiments were carried out under the optimized condition. As shown in Figure 4, TCPB-Zr-NS can effectively drive the

Table 2: The scope of cyclization of o-phenylenediamine derivatives with CO_2 as a C_1 source.[a]

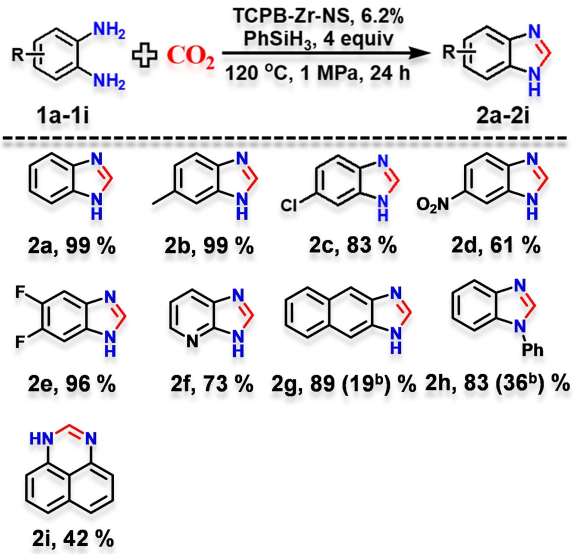

[a] The reactions were performed in a PTFE-lined autoclave (20 mL) with **1** (0.2 mmol), $PhSiH_3$ (0.8 mmol), and TCPB-Zr-NS (6.2 % mol, based on B centers) in ACN (2.0 mL) under CO_2 (1.0 MPa) atmosphere. [b] Catalyst-TCPB-Zr-3D. Isolated yield.

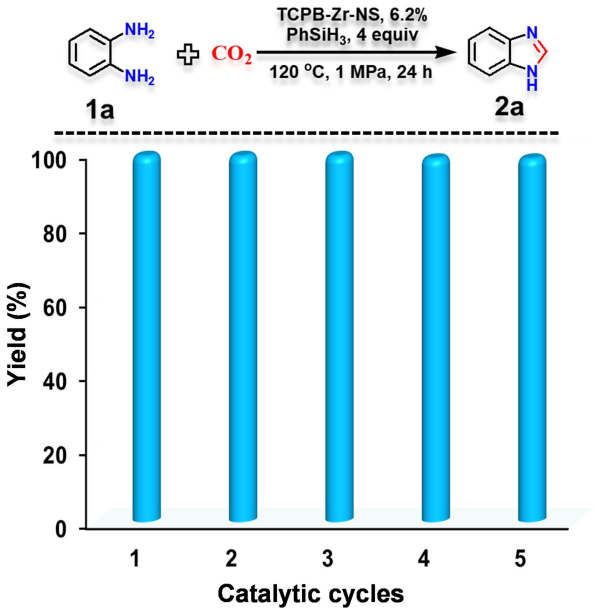

Figure 4. The cycled catalytic performance of TCPB-Zr-NS.

cyclization reaction in five runs, verified by the PXRD, N_2 adsorption, NMR, HR-TEM images, and elemental mappings after the fifth catalytic cycle, corroborating the excellent reusability/durability of TCPB-Zr-NS (Figures S5, S9, S12, S25, and Table S2).

To probe the underlying catalytic reaction mechanism, the X-ray photoelectron spectroscopy (XPS) was performed for TCPB-Zr-NS and 1a@TCPB-Zr-NS (1a@TCPB-Zr-NS represents TCPB-Zr-NS after loading the substrate, **1a**), which revealed no obvious difference for both samples, suggesting no direct interactions between the B centers and amino groups ascribed to the large steric hindrance of duryl groups and rigidity of TCPB-Zr-NS, further confirmed by the solid-state ^{11}B CP/MAS NMR spectra (Figures S23–S24). The isostructural BTB–Zr bearing Zr ions and formates, was selected to perform the cyclization of o-phenylenediamine with CO_2 under the optimized condition, which resulted in marginal benzimidazole product, precluding the effect of Zr ions and formates.[50,58] Since the microporous feature of BTB–Zr may affect the substrate/product diffusion, another Zr_6-cluster based MOF, NU-1000,[60] featuring the same Zr_6 cluster and mesoporous channel (~3.1 nm), was chosen to perform the cyclization reaction, revealing a yield of 29 %, further excluding the effect of Zr ions (Table S3, Entry 15). Besides, the cyclization of o-phenylenediamine with CO_2 under the optimized condition proceeded poorly in absence of TCPB-Zr-NS, precluding the possibility of substrate self-catalyzed reaction (Table S3, Entry 11). To assess the role of B centers, the cyclization reaction was performed under the optimized conditions using TCPB-Zr-NS treated with excess NaF as the catalyst, which revealed a significantly decreased yield of 53 %, suggesting the vital role of B centers for the activation of CO_2 (Table S3, Entry 14). To examine the effect of formate, TCPB-Zr-NS was treated with diluted HCl DMF solution at 70 °C for 24 h to remove partial formates coordinated to the Zr_6 cluster. The result showed that TCPB-Zr-NS treated with diluted HCl presented slightly decreased benzimidazole yield of 88 %, indicative of the auxiliary function of formates in the cyclization reaction (Table S3, Entry 13). Note that the cyclization of o-phenylenediamine with CO_2 can be driven by LA via formylation transfer from formamides, such as DMF or *N*-formylmorpholine, to o-phenylenediamine followed by cyclization of the *N*-formylated intermediate, wherein the formylation of anilines is the key challenge due to their poor nucleophilicity.[61–63] Although the quintessential strong Lewis acid, $B(C_6F_5)_3$, has been utilized as a LA catalyst for formylation transfer and the subsequent condensation of *N*-(2-aminophenyl)formamide to benzimidazole, it is also known to be incompetent for achieving efficient *N*-formylation of o-phenylaniline.[64] Therefore, we suppose that the duryl group decorated organoborane with weaker acidity also is incompetent for the similar reactivity. Indeed, we didn't detect the intermediate, *N*-(2-aminophenyl)formamide, during the cyclization process when using TCPB-Zr-NS as the catalyst. Based on the above results, a LA catalyzed cyclization mechanism was precluded. Moreover, the ^{1}H NMR analysis revealed the ratio of Zr_6-cluster: TCPB: FA of approximately 1: 2: 5, therefore each formate mainly adopted usual coordination mode, in which the O atoms of formate was ligated by two adjacent Zr ions (Figures S4, S26). Considering the ability of carboxylate to activate $PhSiH_3$ to facilitate CO_2 reductive cyclization with o-phenylenediamine,[65–66] the vast distances between B and formate in TCPB-Zr-NS (8.95, 10.80, 12.40, and 12,67 Å, Figure S26), and the efficient reactivity in the presence of both B sites and formates, thus a dynamically liberated formate-assisted FLP-mediated catalytic mechanism different from previously reported mechanism[17–20] was proposed (Figure 5). To further gain insight into the

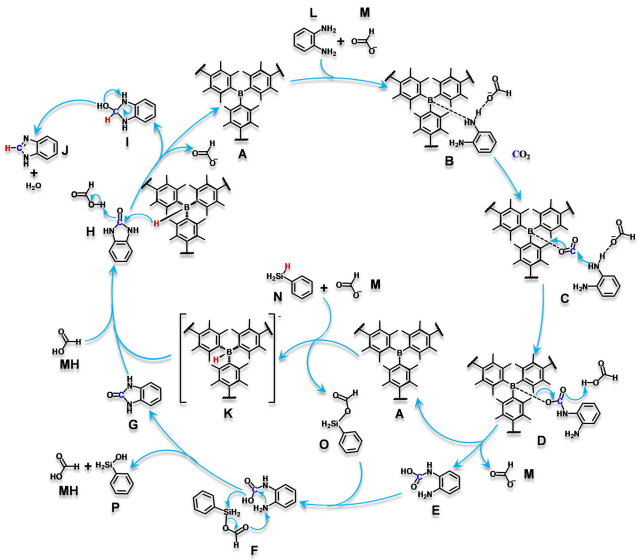

Figure 5. The proposed catalytic mechanism for the cyclization of o-phenylenediamine with CO_2 by TCPB-Zr-NS.

catalytic mechanism, functional density theory (DFT-D) calculation was carried out (computational details can be found in Supporting Information, section 13), in which the corresponding Gibbs free energies based on the proposed reaction pathway were discussed (Figure 6).[67–71] Tri(phenylduryl)borane (TPB) arising from TCPB-Zr-NS was chosen to implement the catalysis calculation to simplify the simulation process (Figure S27). As shown in Figures 5 & 6, the B centers from TCPB-Zr-NS react firstly with o-phenylenediamine to deliver intermediates, B, under the assistant of formate, which further activate CO_2 via FLP-mediated mode to form C, with a Gibbs free energy barrier of 9.03 kcal mol^{-1}. The proton migration combined with C–O activation occurs to produce D, accompanying with released Gibbs free energy of 5.56 kcal mol^{-1}. Thereafter, protonation of the carbamate by formic acid (FA) coincided with cleavage of the B—O interactions happen to afford carbamic acid, E, and regenerated A and formate, during which a transition state, TS1, can be searched with the activated Gibbs free energy lying at 16.87 kcal mol^{-1}. Concurrently, the reductant, $PhSiH_3$, is activated by B centers under the assistant of formate to generate the $[LAH]^-$ intermediates, K, and $PhSiH_2$-formate, O, which further reacts with E to form F. Notably, for the $PhSiH_3$ activation process, a transition state, TS4, is searched with a free energy barrier of 15.12 kcal mol^{-1}. Nucleophilic attack by the amine on the carbamic acid carbon coupled with OH^- abstraction in intermediate F occur accompanying with $PhSiH_2OH$ and FA releasing, generating a benzimidazolone intermediate, G. In this step, the second transition state, TS2, is searched with a free energy barrier of 18.91 kcal mol^{-1}. Subsequently, the hydrogenation of ketone, G, with K and FA occur via a FLP-like activation mode involving "simultaneously" H^+ and H^- transfer to deliver the benzimidazol-ol intermediate, I. Finally, the hydrolysis of the benzimidazol-ol intermediate occurs through a transition state, TS3, with a free energy barrier of 10.41 kcal mol^{-1}, to afford the product, benzimidazole. Overall, the calculated Gibbs free energy curve verifies the feasibility of the cyclization reaction between o-phenylenediamine and CO_2 in the presence of TCPB-Zr-NS with $PhSiH_3$ as the reductant via a formate-assisted FLP-mediated catalytic pathway.

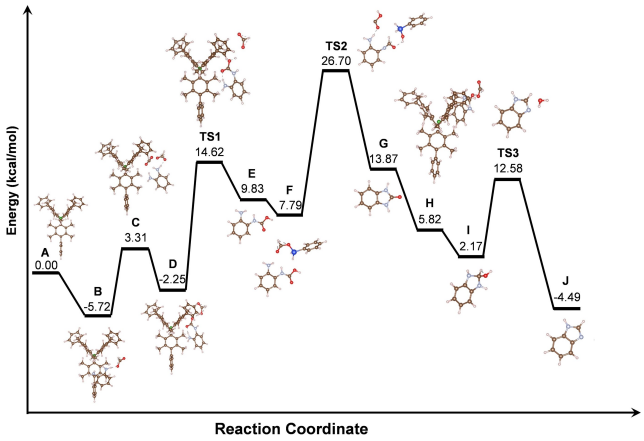

Figure 6. The DFT calculated Gibbs free energetic curve for the cyclization reaction of o-phenylenediamine with CO_2 using TCPB-Zr-NS as the catalyst.

Conclusions

In summary, a robust organoboron functionalized Zr-MON, TCPB-Zr-NS, featuring an abundance of highly exposed Lewis acidic B and formate centers, has been successfully constructed, for efficient CO_2 conversion. Significantly, the synthesized TCPB-Zr-NS showcases dramatically improved catalytic performance for the conversion of o-phenylenediamines to high-valued benzimidazole derivatives by use of CO_2 as a C_1 source compared with the parent TCPB-Zr-3D due to the high exposed active sites and efficient substrates/products diffusion. The high stability endows TCPB-Zr-NS with excellent recyclability and durability confirmed by the consecutive catalytic experiments operated under ambient conditions. The underlying catalytic mechanism is well established by the experiments and DFT-D theoretical calculations, in which a formate-assisted FLP-mediated catalysis pathway occurs in the cyclization reaction of o-phenylenediamine and CO_2. This work may shed light on the future design and construction of robust B-functionalized MON materials for CO_2-conversion-based applications via FLP-mediated catalytic mode.

An organoboron functionalized ultra-thin metal-organic nanosheet, termed TCPB-Zr-NS, featuring highly exposed Lewis acidic B and formate sites, and efficient substrates/products diffusion ability, which presents dramatically improved CO_2 conversion to bioactive benzimidazoles via formate-assisted FLP-mediated catalysis pathway than the parent TCPB-Zr-3D counterpart.

Acknowledgements

The authors acknowledge the financial support from the Robert A. Welch Foundation (B-0027) for this work. Partial support from NSFC (22001271) (CXC) and Researchers Supporting Program (RSP2025R79) at King Saud University, Riyadh, Saudi Arabia (AN) is also acknowledged. HR thanks University of North Texas and the CASCaM facility for the computing resources (OAC-2117247).

Conflict of Interest

The authors declare no conflict of interest.

Data Availability Statement

The data that support the findings of this study are available from the corresponding author upon reasonable request.

Keywords: metal-organic nanosheets · frustrated Lewis pair · organoborane linker · CO_2 conversion · heterogeneous catalysis

[1] H. Zhou, R. Zhang, X.-B. Lu, *Adv. Synth. Catal.* **2019**, *361*, 326–334.
[2] A. George, B. Shen, M. Craven, Y. Wang, D. Kang, C. Wu, X. Tu, *Renewable Sustainable Energy Rev.* **2021**, *135*, 109702–109782.
[3] X. Zhang, J. Sun, G. Wei, Z. Liu, H. Yang, K. Wang, H. Fei, *Angew. Chem. Int. Ed.* **2019**, *58*, 2844–2849.
[4] J. Artz, T. E. Müller, K. Thenert, J. Kleinekorte, R. Meys, A. Sternberg, A. Bardow, W. Leitner, *Chem. Rev.* **2018**, *118*, 434–504.
[5] J. Wei, Q. Ge, R. Yao, Z. Wen, C. Fang, L. Guo, H. Xu, J. Sun, *Nat. Commun.* **2017**, *8*, 15174.
[6] X. D. Lang, L. N. He, *ChemSusChem* **2018**, *11*, 2062–2067.
[7] A. Velty, A. Corma, *Chem. Soc. Rev.* **2023**, *52*, 1773–1946.
[8] J. R. Cabrero-Antonino, R. Adam, M. Beller, *Angew. Chem. Int. Ed.* **2019**, *58*, 12820–12838.
[9] F. Zhang, Y. Wang, X. Zhang, X. Zhang, H. Liu, B. Han, *Green Chem. Eng.* **2020**, *1*, 82–93.
[10] R. R. Shaikh, S. Pornpraprom, V. D'Elia, *ACS Catal.* **2018**, *8*, 419–450.
[11] A.-L. Gu, Y.-X. Zhang, Z.-L. Wu, H.-Y. Cui, T.-D. Hu, B. Zhao, *Angew. Chem. Int. Ed.* **2022**, *61*, e202114817.
[12] S. Arshadi, E. Vessally, M. Sobati, A. Hosseinian, A. Bekhradnia, *J. CO_2 Util.* **2017**, *19*, 120–129.
[13] R. Huang, J. Rintjema, J. González-Fabra, E. Martín, E. C. Escudero-Adán, C. Bo, A. Urakawa, A. W. Kleij, *Nat. Catal.* **2019**, *2*, 62–70.
[14] J. Hong, M. Li, J. Zhang, B. Sun, F. Mo, *ChemSusChem* **2019**, *12*, 1–35.
[15] M. Ding, R. W. Flaig, H.-L. Jiang, O. M. Yaghi, *Chem. Soc. Rev.* **2019**, *48*, 2783–2828.
[16] E. Nikoloudakis, I. López-Duarte, G. Charalambidis, K. Ladomenou, M. Ince, A. G. Coutsolelos, *Chem. Soc. Rev.* **2022**, *51*, 6965–7045.
[17] Y. Sun, K. Gao, *J. Org. Chem.* **2023**, *88*, 7463–7468.
[18] S. Shyshkanov, T. N. Nguyen, F. M. Ebrahim, K. C. Stylianou, P. J. Dyson, *Angew. Chem. Int. Ed.* **2019**, *58*, 5371–5375.
[19] C.-X. Chen, H. Rabaâ, H. Wang, P. C. Lan, Y.-Y. Xiong, Z.-W. Wei, A. M. Al-Enizi, A. Nafady, S. Ma, *CCS Chem.* **2023**, *5*, 1989–1998.
[20] A. Dai, S. Li, T. Wang, Y. Yang, Y. Tian, X. Jing, G. Zhu, *Chin. Chem. Lett.* **2023**, *34*, 107559.
[21] Y. Ma, S. Zhang, C.-R. Chang, Z.-Q. Huang, J. C. Ho, Y. Qu, *Chem. Soc. Rev.* **2018**, *47*, 5541–5553.
[22] J. Lam, K. M. Szkop, E. Mosaferi, D. W. Stephan, *Chem. Soc. Rev.* **2019**, *48*, 3592–3612.
[23] X. Feng, W. Meng, H. Du, *Chem. Soc. Rev.* **2023**, *52*, 8580–8598.
[24] Y. Zhang, P. C. Lan, K. Martin, S. Ma, *Chem Catal.* **2022**, *2*, 439–457.
[25] T. Wang, M. Xu, A. R. Jupp, Z. W. Qu, S. Grimme, D. W. Stephan, *Angew. Chem. Int. Ed.* **2021**, *60*, 25771–25775.
[26] J. Paradies, *Eur. J. Org. Chem.* **2019**, *2019*, 283–294.
[27] D. W. Stephan, *Science* **2016**, *354*, 1248–1256.
[28] D. W. Stephan, *Acc. Chem. Res.* **2015**, *48*, 306–316.
[29] J. Chen, L. Falivene, L. Caporaso, L. Cavallo, E. Y. X. Chen, *J. Am. Chem. Soc.* **2016**, *138*, 5321–5333.
[30] Z. Yang, B. Yu, H. Zhang, Y. Zhao, G. Ji, Z. Ma, X. Gao, Z. Liu, *Green Chem.* **2015**, *17*, 4189–4193.
[31] M. A. Courtemanche, M. A. Legare, L. Maron, F. G. Fontaine, *J. Am. Chem. Soc.* **2014**, *136*, 10708–10717.
[32] L. Chen, R. Liu, Q. Yan, *Angew. Chem. Int. Ed.* **2018**, *57*, 9336–9340.
[33] C. M. Mömming, E. Otten, G. Kehr, R. Fröhlich, S. Grimme, D. W. Stephan, G. Erker, *Angew. Chem. Int. Ed.* **2009**, *121*, 6770–6773.
[34] Q. Liu, Q. Liao, J. Hu, K. Xi, Y.-T. Wu, X. Hu, *J. Mater. Chem. A* **2022**, *10*, 7333–7340.
[35] Q. Meng, Y. Huang, D. Deng, Y. Yang, H. Sha, X. Zou, R. Faller, Y. Yuan, G. Zhu, *Adv. Sci.* **2020**, *7*, 2000067–2200075.
[36] W. Chen, S. Li, L. Yi, Z. Chen, Z. Li, Y. Wu, W. Yan, F. Deng, H. Deng, *J. Am. Chem. Soc.* **2024**, *146*, 12215–12224.
[37] Z. Hu, Z.-W. Fan, Z.-M. Xu, Y. Wu, H.-W. Zhang, Y.-L. Huang, Z. Niu, *J. Am. Chem. Soc.* **2024**, *146*, 17924–17930.
[38] S. Das, R. Laplaza, J. T. Blaskovits, C. Corminboeuf, *J. Am. Chem. Soc.* **2024**, *146*, 15806–15814.
[39] E. A. Latif, J. D. Hilgar, N. A. Romero, *J. Am. Chem. Soc.* **2024**, DOI: 10.1021/jacs.4c09012.
[40] Z. Niu, W. Zhang, P. C. Lan, B. Aguila, S. Ma, *Angew. Chem. Int. Ed.* **2019**, *58*, 7420–7424.
[41] Z. Niu, W. D. C. Bhagya Gunatilleke, Q. Sun, P. C. Lan, J. Perman, J.-G. Ma, Y. Cheng, B. Aguila, S. Ma, *Chem* **2018**, *4*, 2587–2599.
[42] Y. Zhang, S. Chen, A. M. Al-Enizi, A. Nafady, Z. Tang, S. Ma, *Angew. Chem. Int. Ed.* **2023**, *62*, e202213399.
[43] Y. Zhang, Y. Jiang, A. Nafady, Z. Tang, A. M. Al-Enizi, K. Tan, S. Ma, *ACS Cent. Sci.* **2023**, *9*, 1692–1701.
[44] Z.-M. Xu, Z. Hu, Y. Huang, S.-J. Bao, Z. Niu, J.-P. Lang, A. M. Al-Enizi, A. Nafady, S. Ma, *J. Am. Chem. Soc.* **2023**, *145*, 14994–15000.
[45] Y. Zhang, J. Guo, P. VanNatta, Y. Jiang, J. Phipps, R. Roknuzzaman, H. Rabaa, K. Tan, T. AlShahrani, S. Ma, *J. Am. Chem. Soc.* **2024**, *146*, 979–987.
[46] M. Zhao, Y. Huang, Y. Peng, Z. Huang, Q. Ma, H. Zhang, *Chem. Soc. Rev.* **2018**, *47*, 6267–6295.
[47] Y. Fan, H. Zheng, S. Labalme, W. Lin, *J. Am. Chem. Soc.* **2023**, *145*, 4158–416.
[48] R.-J. Wei, P.-Y. You, H. Duan, M. Xie, R.-Q. Xia, X. Chen, X. Zhao, G.-H. Ning, A. I. Cooper, D. Li, *J. Am. Chem. Soc.* **2022**, *144*, 17487–17495.
[49] J. Nicks, K. Sasitharan, R. R. R. Prasad, D. J. Ashworth, J. A. Foster, *Adv. Funct. Mater.* **2021**, *31*, 2103723.
[50] Y. Wang, L. Feng, J. Pang, J. Li, N. Huang, G. S. Day, L. Cheng, H. F. Drake, Y. Wang, C. Lollar, J. Qin, Z. Gu, T. Lu, S. Yuan, H.-C. Zhou, *Adv. Sci.* **2019**, *6*, 1802059.
[51] J. Duan, Y. Li, Y. Pan, N. Behera, W. Jin, *Coord. Chem. Rev.* **2019**, *395*, 25–45.
[52] W. Shi, L. Cao, H. Zhang, X. Zhou, B. An, Z. Lin, R. Dai, J. Li, C. Wang, W. Lin, *Angew. Chem. Int. Ed.* **2017**, *56*, 9704–9709.
[53] Z.-R. Tao, J.-X. Wu, Y.-J. Zhao, M. Xu, W.-Q. Tang, Q.-H. Zhang, L. Gu, D.-H. Liu, Z.-Y. Gu, *Nat. Commun.* **2019**, *10*, 2911.
[54] Z. Hu, E. M. Mahdi, Y. Peng, Y. Qian, B. Zhang, N. Yan, D. Yuan, J.-C. Tan, D. Zhao, *J. Mater. Chem. A* **2017**, *5*, 8954–8963.
[55] Z. Cheng, J. Lian, Y. Chen, Y. Tang, Y. Huang, J. Zhang, S. Xiang, Z. Zhang, *CCS Chem.* **2023**, *6*, 988–998.
[56] H.-X. Zhang, C. Lu, J. Zhang, *Acc. Mater. Res.* **2023**, *4*, 995–1007.
[57] Q. Xia, J. Zhang, X. Chen, C. Cheng, D. Chu, X. Tang, H. Li, Y. Cui, *Coord. Chem. Rev.* **2021**, *435*, 213783.
[58] R. Wang, Z. Wang, Y. Xu, F. Dai, L. Zhang, D. Sun, *Inorg. Chem.* **2014**, *53*, 7086–7088.
[59] J. Ma, A. G. Wong-Foy, A. J. Matzger, *Inorg. Chem.* **2015**, *54*, 4591–4593.
[60] T. C. Wang, N. A. Vermeulen, I. S. Kim, A. B. F. Martinson, J. F. Stoddart, J. T. Hupp, O. K. Farha, *Nat. Protoc.* **2016**, *11*, 149–162.

[61] M. Faheem, A Rathaur, A. Pandey, V. Kumar Singh, A. K. Tiwari, *ChemistrySelect* **2020**, *5*, 3981–3994.
[62] D. B. Nale, B. M. Bhanage, *Synlett* **2015**, *26*, 2835–2842.
[63] J. Zhu, Z. Zhang, C. Miao, W. Liu, W. Sun, *Tetrahedron* **2017**, *73*, 3458–3462.
[64] M. Hulla, S. Nussbaum, A. R. Bonnin, P. J. Dyson, *Chem. Commun.* **2019**, *55*, 13089–13092.
[65] Z. Ye, J. Chen, *ACS Catal.* **2021**, *11*, 13983–13999.
[66] W. Zhao, H. Li, Y. Li, J. Long, Y. Xu, S. Yang, *Sustainable Chem. Pharm.* **2020**, *17*, 100276–100282.
[67] S. Grimme, J. Antony, S. Ehrlich, H. Krieg, *J. Chem. Phys.* **2010**, *132*, 154104–154122.
[68] G. Kresse, J. Furthmüller, *Comput. Mater. Sci.* **1996**, *6*, 15–50.
[69] G. Kresse, D. Joubert, *Phys. Rev. B* **1999**, *59*, 1758–1775.
[70] J. P. Perdew, K. Burke, M. Ernzerhof, *Phys. Rev. Lett.* **1996**, *77*, 3865–3868.
[71] D. J. Chadi, *Phys. Rev. B* **1977**, *16*, 1746–1747.

Manuscript received: August 28, 2024
Accepted manuscript online: January 13, 2025
Version of record online: ■■, ■■

Research Article

CO_2 Conversion

C.-X. Chen, H. Wang, H. Rabaâ, Y.-Y. Xiong, P. VanNatta, Z.-W. Wei, A. M. Al-Enizi, A. Nafady, S. Ma* _____ **e202416497**

Organoboron-Functionalized Metal-Organic Nanosheets for Highly Efficient CO_2 Fixation Mediated by Frustrated Lewis Pairs

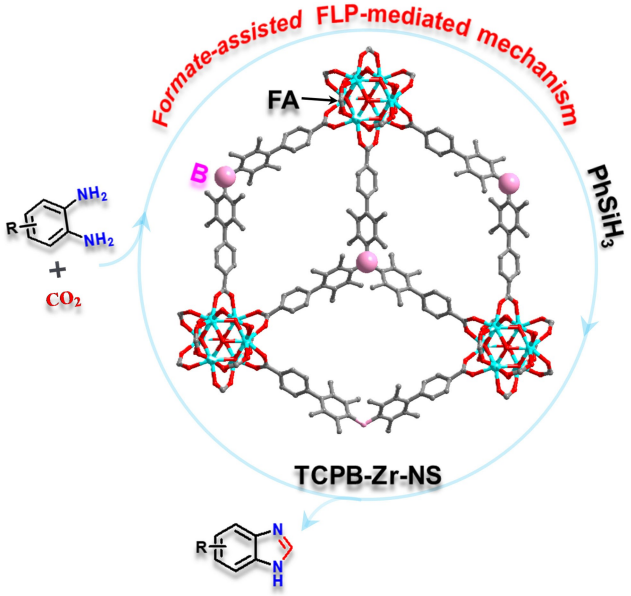

An organoboron functionalized ultrathin metal-organic nanosheet, termed TCPB-Zr-NS, featuring highly exposed Lewis acidic B and formate sites, and efficient substrates/products diffusion ability, which presents dramatically improved CO_2 conversion to bioactive benzimidazoles via formate-assisted FLP-mediated catalysis pathway than the parent TCPB-Zr-3D counterpart.